Multispectral Reconstruction from Single RGB Image Based on Camera Response Expansion and Local Inverse Distance Weighted Optimization

Jinxing Liang, Xiaoxia Wan
School of Printing and Packaging, Wuhan University, Wuhan, China

Abstract

Multispectral reconstruction from single RGB image can eliminate the geometric distortion problem existing in optical bandpass filters-based multispectral cameras and save the capturing time, but the reconstruction accuracy is limited by just using the original three channels response. Camera response expansion is an optimal choice to increase the dimensions of the input information for multispectral reconstruction as the imaging and processing is practically not linearity for the trichromatic digital cameras. In this paper, the camera response expansion based on polynomial model was tested for multispectral reconstruction from single RGB image, the pseudoinverse method was adopted for the training-based multispectral reconstruction, and the local inverse distance weighted (LIDW) optimization was proposed to improve the reconstruction accuracy. The proposed method was compared with the current existing methods through practical experiment, and the results indicated that it outperformed existing methods.

Introduction

Multispectral imaging techniques are developing rapidly in the domains of remote sensing,[1] color imaging,[2] biometrics and medicine,[3] cultural heritage and artwork studies[4] because of their high-quality imaging in colorimetric and spectral aspects. Different multispectral imaging systems have been devised to encompass this wide range of applications, such as digital cameras combined with line-scan spectrographs,[5] color filter wheels,[6] broadband filters,[7] narrowband filters,[8] multiple light sources,[9] and tunable filters of liquid crystal technology.[10] Reflectance reconstruction is a key issue for most of the above optical bandpass filters-based multispectral system as it is an ill-posed problem solution for high-dimensional reflectance estimation from the low-dimensional multi-channel digital response, and has been extensively studied.[11-13] Besides, the geometric distortion, which reduces the multispectral imaging accuracy, is an inherent problem for optical bandpass filters-based multispectral system and is difficult to calibrate and correct because of the complexity of optical imaging systems.[14] Rethinking of the principal of the current available optical bandpass filters-based multispectral system, the main advantages of these system compared with the traditional trichromatic digital imaging devices is that they have more response channels, and therefore generates more dimensions of the response signal. Inspired by this finding, we intend to reconstruct the multispectral image from single RGB image based on the concept of camera response expansion, which could effectively overcome the geometric distortion problem, and at the same time save the capturing period.

In this paper, the camera response expansion basing on polynomial model was tested for multispectral reconstruction from single RGB image. The trichromatic digital camera response was firstly expanded to more items than the original three channels, and the spectral reflectance was reconstructed from the expanded camera response using the training-based pseudoinverse reflectance reconstruction method. The LIDW optimization method was proposed to improve the reconstruction accuracy. The influences of the number of local training samples and the number of expansion items on reconstruction accuracy was explored, and the optimal number of local training samples and response expansion items were determined. The proposed method was compared with the current existing methods under the premise of all these methods using their optimal parameters, including PLS method,[15] SR-LLA method,[16] PCA-based method,[17] the method proposed by Cao et al.,[13] and the method proposed method by Zhang et al..[18]

The paper is organized as follows. In Sec. 2 we give a short introduction about the current available multispectral systems, the advantages and the principal of multispectral reconstruction from the single RGB image. Sec. 3 depicts the system model of digital camera and the multispectral reconstruction method whereas the experiment results are shown and discussed in Sec. 4. In Sec. 5 we finish the paper with some concluding remarks and an outlook on future developments.

System and methodology

System model and multispectral reconstruction methods

Supposing a linear optoelectronic transfer function of the trichromatic digital camera,[10] the response of the digital camera can be formulated by the equation:

$$d_i = \int_{\lambda_{\min}}^{\lambda_{\max}} l(\lambda) s_i(\lambda) o(\lambda) r(\lambda) d\lambda + b_i + n_i \,, \tag{1}$$

where the camera response d_i is related to the channel i of a sample or a pixel in the image, λ is wavelength, ranging from $\lambda_{\min}$ to $\lambda_{\max}$ in visible wavelength range, $l(\lambda)$ is the relative spectral radiance of the illuminant, $s_i(\lambda)$ is the spectral sensitivity of the ith channel of the camera, $o(\lambda)$ is the spectral transmittance of the camera optical system, $r(\lambda)$ is the spectral reflectance of a sample or a pixel in the image, *bi* and *ni* are the mean zero Gaussian white noise and the dark current noise of the ith channel in the digital camera respectively, which are often ignored for simplicity. The Eq. (1) can be written in matrix notation as follows:

$$\mathbf{d} = \mathbf{Mr}\ , \tag{2}$$

where **d** is the response vector of a sample or a pixel in the image, **M** is the overall spectral sensitivity matrix of the camera imaging system including the product of the matrix form of $l(\lambda)$, $s_i(\lambda)$, and $o(\lambda)$, and **r** denotes the spectral reflectance vector of a sample or a pixel in the image. For multispectral reconstruction, the goal is to reconstruct the high-dimensional reflectance $\mathbf{r}_{\mathbf{rec}}$ from the low-dimensional camera response vector **d** by:

$$\mathbf{r}_{\mathbf{rec}} = \mathbf{Qd}\ . \tag{3}$$

The accuracy of reflectance reconstruction is determined by the method of solving the transformation matrix **Q**. If the spectral sensitivity matrix **M** is accurately characterized before the reflectance reconstruction, the $\mathbf{r}_{\mathbf{rec}}$ can be directly reconstructed from **d** using pseudoinverse, PCA or Wiener estimation method.[13] However, in most instances, it is hard and inconvenient to characterize the matrix **M** instrumentally as several imaging system parameters are included in it. Therefore, the training-based pseudoinverse method is widely selected by most studies as shown in Eq. (4), where the superscript + is the pseudoinverse operator, the $\mathbf{R}_{\mathbf{train}}$ denotes the reflectance matrix of the training sample set, and $\mathbf{D}_{\mathbf{train}}$ represents the camera response matrix of the training sample set. The training-based pseudoinverse multispectral reconstruction method is also used in this paper.

$$\mathbf{r}_{\mathbf{rec}} = \mathbf{R}_{\mathbf{train}}\mathbf{D}_{\mathbf{train}}^{+}\mathbf{d}\ . \tag{4}$$

Proposed method

As pointed by previous studies, reflectance reconstruction accuracy was limited by just using the original three channels response.[19, 20] However, except for the methods of increasing the imaging channels in multispectral system, the method of increasing the camera response items by expanding the original three channels response was also proved to be an effective method.[13,15-18] In Eq. (1), we assume the imaging process is ideal linearity for trichromatic digital camera, but this is not true for practical digital imaging process as the image-enhancement step is non-linear and difficult to simulate.[21] Therefore, the polynomial model which had been applied for the color correction and characterization of color imaging device, was applied as the referenced model for camera response expansion. The fourth-order polynomial model including 35 items, as shown in Eq. (5), was selected as the basic referenced model for camera response expansion in this paper.

$$\begin{aligned}\mathbf{d}_{\mathbf{expanded}} = [&1\ r\ g\ b\ rg\ rb\ gb\ r^2\ g^2\ b^2\ rg^2\ r^2g\ rb^2\ r^2b \\ &gb^2\ g^2b\ r^3\ g^3\ b^3\ rgb\ rg^3\ r^2g^2\ rg^3\ rb^3\ r^2b^2 \\ &r^3b\ gb^3\ g^2b^2\ r^3b\ r^2gb\ rg^2b\ rgb^2\ r^4\ g^4\ b^4]\end{aligned} \tag{5}$$

Where $\mathbf{d}_{\mathbf{expanded}}$ is the expanded response vector, and *r*, *g* and *b* are the response values of the R-channel, G-channel, and B-channel of the trichromatic digital camera. However, if all items of the expanded response in Eq. (5) are used for multispectral reconstruction, it may lead to the over-fitting problems as explained in literature.[22] Thus, the optimal number of response expansion items should be determined before the formal reflectance reconstruction. The method of traversal all possible situations of response expansion to determine the optimal number of response expansion was adopted in this paper as shown in Eq. (6).

$$\begin{aligned}&4\,items\!: \ \mathbf{d}_{\mathbf{expanded}} = [1\ r\ g\ b], \\ &5\,items\!: \ \mathbf{d}_{\mathbf{expanded}} = [1\ r\ g\ b\ rg], \\ &6\,items\!: \ \mathbf{d}_{\mathbf{expanded}} = [1\ r\ g\ b\ rg\ rb], \\ &\ \vdots \qquad\quad \vdots \qquad\qquad \vdots \\ &35\,items\!: \mathbf{d}_{\mathbf{expanded}} = [1\ r\ g\ b\ rg\ rb\ gb\ r^2\ g^2\ b^2\ rg^2\ r^2g\ rb^2\ r^2b\ gb^2 \\ &\qquad g^2b\ r^3\ g^3\ b^3\ rgb\ \ rg^3\ r^2g^2\ rg^3\ rb^3\ r^2b^2\ r^3b \\ &\qquad gb^3\ g^2b^2\ r^3b\ r^2gb\ rg^2b\ rgb^2\ r^4\ g^4\ b^4]\end{aligned} \tag{6}$$

It is known that the spectral or chromatic similarity between training samples set and test targets determines the reconstruction accuracy, the higher the similarity, the better the reconstruction accuracy, and vice versa.23 Furthermore, too many samples in the training set may lead to color or spectral information redundancy, which would increase the computation time and slightly decrease the reconstruction accuracy as shown in Figure 2(a). Therefore, the LIDW optimization method was proposed to improve the reconstruction accuracy. Firstly, the euclidean distance between the test samples and the training samples are calculated in RGB color space as shown in Eq. (7):

$$e_j = \sqrt{(r_{test} - r_j)^2 + (g_{test} - g_j)^2 + (b_{test} - b_j)^2}\quad (j = 1, 2, \cdots, N)\,, \tag{7}$$

where subscript *j* is the *j*th sample in the training sample set, e_j is the euclidean distance between the jth training sample and the test sample, and *N* is the number of samples in training sample set. Then, the training samples were sorted in ascending order according to their distance with the test sample. The first *p* ($1 \le p \le N$) samples were extracted as the local optimal sample set, and the inverse distance weighted coefficient w_{k} was calculated for each of the selected local optimal samples as shown in Eq. (8):

$$w_k = \frac{1}{e_k + \varepsilon}\quad (k = 1, 2, \cdots, p)\,, \tag{8}$$

where subscript *k* is the *k*th sample in local optimal sample set, e_k is the euclidean distance between the *k*th local optimal training sample and the test sample, ε is a very small value added to avoid zero divided in Eq. (8), ε = 0.001 is used in this paper. The weighted matrix **W** can be written as:

$$\mathbf{W} = \begin{bmatrix} w_1 & 0 & \cdots & 0 \\ 0 & w_2 & 0 & \vdots \\ \vdots & 0 & \ddots & 0 \\ 0 & \cdots & 0 & w_p \end{bmatrix}_{p\times p}\ . \tag{9}$$

At last, the spectral reflectance of the test sample was reconstructed as follows:

$$\mathbf{r}_{\mathbf{test}} = \mathbf{W}\mathbf{R}_{\mathbf{localtrain}}(\mathbf{W}\mathbf{D}_{\mathbf{localtrain}})^{+}\mathbf{d}_{\mathbf{testexpanded}}\ , \tag{10}$$

where $\mathbf{r}_{test}$ is the reconstructed spectral reflectance vector of the test sample, $\mathbf{R}_{localtrain}$ is the reflectance matrix of the selected local optimal samples, $\mathbf{D}_{localtrain}$ is the expanded response matrix of the selected local optimal samples, and $\mathbf{d}_{testexpanded}$ is the expanded response vector of the test sample.

Experiment

In this paper, a mineral pigment color book including 784 color patches was used to verify the proposed methods. The spectral reflectance of the sample set was measured with the X-rite Eye One Pro spectrophotometer at 10nm intervals from 400 to 700nm. The odd number samples are selected as training set to reconstruct the even number testing samples. The chromaticity coordinates of the training and testing samples in CIELab color space calculated using D50 illumination and CIE1931 standard observer functions are plotted in Figure 1(a) and Figure 1(b), respectively.

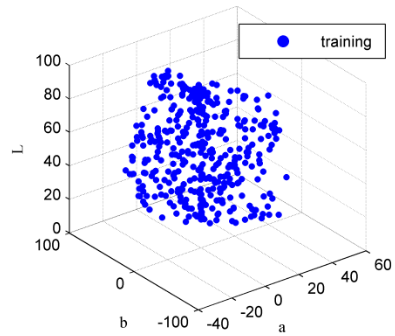

(a)

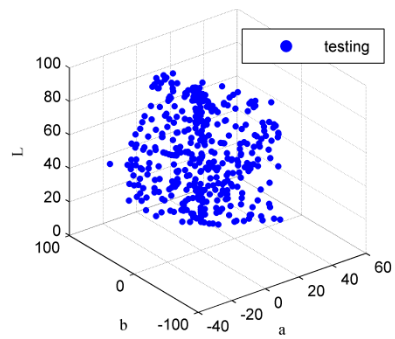

(b)

Figure 1. Chromaticity distribution of samples: (a) training samples, (b) testing samples.

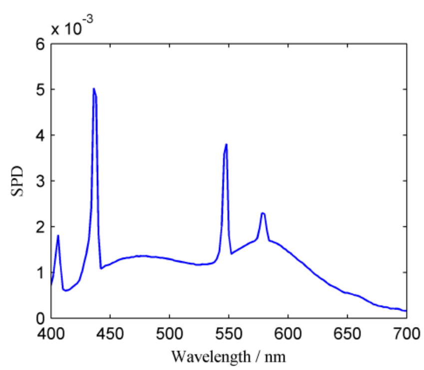

Figure 2. The relative spectral power distribution of the flat fluorescent lamp.

The digital image of the samples was captured with a Canon 600D trichromatic digital camera in the normal direction under the illumination of a flat fluorescent lamp at an angle of 45°. The relative spectral power distribution (SPD) of the flat fluorescent lamp measured with the PR705 spectroradiometer and the Spectralon® standard whiteboard is plotted in Figure 2. The parameters set for the camera were fixed during the experiment, with the aperture size was set to 3.5, the exposure time was 1/40 second, and the ISO was 100. The dark current noise was recorded with the camera lens cap closed and was subsequently subtracted from the images. The illumination uniformity was corrected using the uniform gray card as described in literature 20. The spectral root-mean-square (RMS) error and the CIEDE2000 color difference (DE_{00}) under D50 illumination and CIE1931 standard observer functions were selected to evaluate the multispectral reconstruction accuracy. The calculation of spectral RMS error is shown in Eq. (11), the superscript T is the transpose operator, $\mathbf{r}_{rec}$ is the spectral reflectance vector of the reconstructed sample, $\mathbf{r}_{ref}$ is the measured reference spectral reflectance vector of the sample, K is the sampling number of spectral reflectance in visible spectrum, for spectral wavelength ranges from 400 to 700nm at 10nm intervals, K = 31. The calculation of the CIEDE2000 color difference can be referred to literature 24.

$$RMS = \sqrt{\frac{1}{K}(\mathbf{r}_{rec} - \mathbf{r}_{ref})^T(\mathbf{r}_{rec} - \mathbf{r}_{ref})}\,. \tag{11}$$

Results and discussion

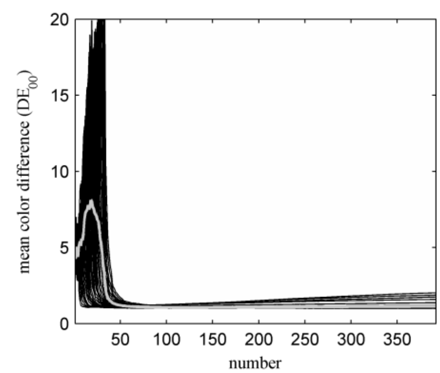

(a)

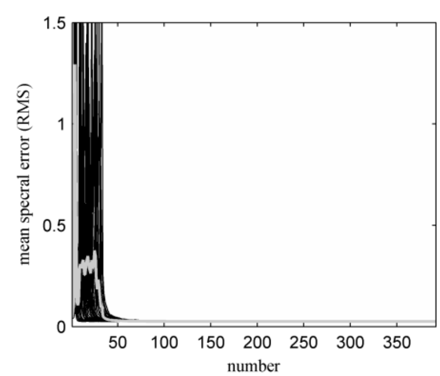

(b)

Figure 3. Relationship between the local number of training samples and reconstruction accuracy in different number of response expansion items from 4 to 35 (thin black line) and the overall average (thick gray line): (a) DE_{00}, (b) RMS.

The influence of the number of local training samples and the number of expansion items on reconstruction accuracy are investigated as shown in Figure 3 and Figure 4. The thin black lines represent the relationship between the number of local training samples or the number of expansion items and the reconstruction errors, and the thick gray line indicates the overall average of the thin black lines. The relationship between the number of local training samples and the corresponding reconstruction errors in different number of response expansion items from 4 to 35 is plotted in Figure 3, the overall average reconstruction errors of the testing samples initially increases and then decreases with the number of local training samples, when the number local training samples reaches to 50, the overall average reconstruction errors began to stabilize, and when the number local training samples reaches to 100, the overall average reconstruction errors has stabilized. But for some small number of camera response expansion items in Figure 3(a), too many local training samples are causing the slightly increases of the mean color difference.

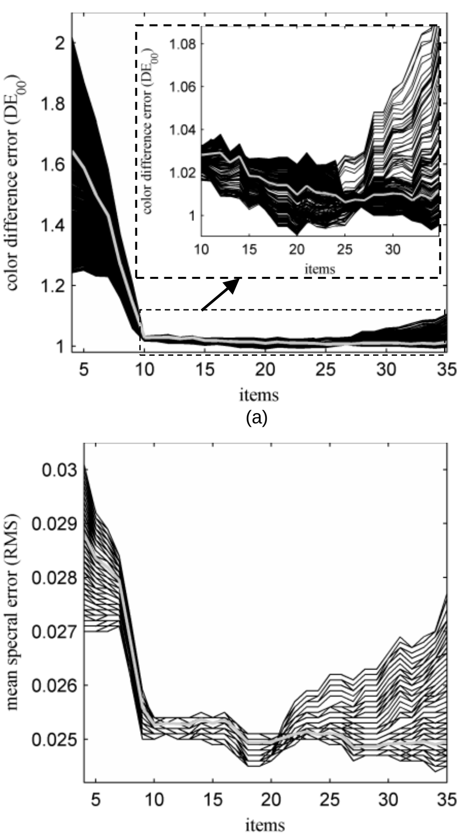

Figure 4. Relationship between the number of response expansion items and reconstruction accuracy in different number of local training samples from 100 to 392 (thin black line) and the overall average (thick gray line): (a) DE_{00}, (b) RMS.

The relationship between response expansion items and the corresponding reconstruction errors in different number of local training samples from 100 to 392 is plotted in Figure 4. With the number of the items, the overall average reconstruction errors initially decrease rapidly, and then decrease slightly when the items reaches to 10. However, when the number of items is greater than 10, the vibration phenomenon occurs for both the color difference and the spectral error as indicate of the insert in Figure 4(a) and the Figure 4(b), which proves that the number of local training samples has an effect on the choice of the optimal number of response expansion items. Simultaneously, the number of response expansion items also has an effect on the choice of the optimal number of local training samples.

According to the above analysis, two optimal combinations of the number of local training samples and number of response expansion items in our proposed method are selected to compare with the current existing methods. The first optimal combination is 100 local training samples and the corresponding 18 response expansion items (named as Proposed-1), while the second optimal combination is 27 response expansion items and the corresponding all 392 local training samples (named as Proposed-2). And all the compared methods also use their optimal parameters for reflectance reconstruction in this paper. The experiment results are summarized in Table 1.

Table 1. Comparison between the proposed method and the current existing methods

	DE_{00}			
	Mean	Median	Max.	Std.
PLS	1.4256	1.1177	7.3434	1.0587
SR-LLA	1.6429	1.3501	14.3672	1.3212
PCA-based	1.4854	1.1993	7.8975	1.0698
Cao	2.9773	2.4797	12.8931	2.1213
Zhang	1.4262	1.1209	7.3488	1.0598
Proposed-1	1.0057	0.8892	3.5445	0.5881
Proposed-2	1.0030	0.8734	3.3959	0.5788
	RMS			
	Mean	Median	Max.	Std.
PLS	0.0303	0.0244	0.1780	0.0235
SR-LLA	0.0357	0.0254	0.4098	0.0386
PCA-based	0.0312	0.0248	0.1776	0.0234
Cao	0.0311	0.0250	0.1646	0.0244
Zhang	0.0333	0.0277	0.1794	0.0228
Proposed-1	0.0246	0.0184	0.1706	0.0235
Proposed-2	0.0247	0.0190	0.1617	0.0226

It can be seen from Table 1 that the proposed method is apparently superior to the other several method for both the color difference and spectral error. The reflectance reconstruction accuracy of the two optimal combinations of the proposed method is very close. Among the current existing methods, the PLS method has the best reconstruction accuracy although it is inferior to the proposed method. The method proposed by Zhang et al. obtains the very close reconstruction accuracy to the PLS method. The PCA-based method also acquires the reasonable reconstruction accuracy, while the SR-LLA method and the method proposed by Cao et al. are bad compared with other methods.

In order to compare the reconstruction accuracy of the above methods more intuitively, the reconstruction error distribution of test samples is counted and plotted in Figure 5. There are more test samples of the proposed method located in the small error interval than other methods. For the proposed method in Figure 5(a), there are 226 test samples smaller than 1 DE_{00}, 389 samples smaller than 3 DE_{00} and on three samples bigger than 3 DE_{00}. However, for the PLS method, the corresponding number are 161, 358 and 34 respectively, the distribution of color difference of other methods is worse. The statistical results about distribution of spectral error in Figure 5(b) are similar to Figure 5(a).The statistical results in Figure 5(a) and Figure 5(b) further illustrates the advantages of the proposed method in this paper.

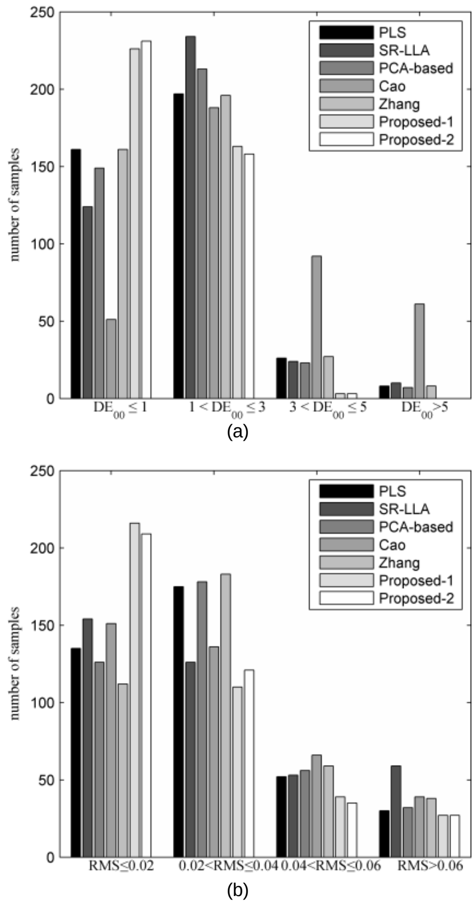

Figure 5. The error distribution of test samples of different methods: (a) distribution of test samples in different color difference (DE_{00}) intervals, and (b) distribution of test samples in different spectral (RMS) error intervals.

Conclusion and outlook

An improved multispectral reconstruction method from single RGB image based on camera response expansion and LIDW optimization is proposed in this paper. The experiment result shows that the proposed method can obtain the reasonable reconstruction accuracy and is apparently superior performance to the current existing methods. Compare to the best the current existing method, the mean and median CIEDE2000 color difference of the proposed improved about 0.4, and the maximum is halved. The mean and median spectral error also acquires a significant improvement. In the future research works, based on the prior knowledge of specific artworks (such as the ancient murals), we will explore the feasibility of non-visible multispectral reconstruction from single RGB image using the proposed method in this paper. And if feasible, more valuable information will be acquired from the RGB image for scientific analysis of artworks.

Acknowledgements

This work was supported by the National Natural Science Foundation of China (Grant no. 61575147, and 61275172).

References

[1] P. Yuen and M. Richardson, An introduction to hyperspectral imaging and its application for security, surveillance and target acquisition, The Imaging Science Journal, 2010, 58(5): 241-253.

[2] S. Tominaga and N. Tanaka, Spectral image acquisition, analysis, and rendering for art paintings, Journal of Electronic Imaging, 2008, 17(4): 043022.

[3] N. L. Everdell, I. B. Styles, E. Claridge, J. C. Hebden, and A. S. Calcagni. Multispectral imaging of the ocular fundus using LED illumination. In Novel Optical Instrumentation for Biomedical Applications IV, volume 7371 of SPIE Proceedings, 2009.

[4] H. Liang, Advances in multispectral and hyperspectral imaging for archaeology and art conservation, Applied Physics A, 2012, 106(2): 309-323.

[5] D. F. Barbin, G. ElMasry, D. W. Sun, and P. Allen, Predicting quality and sensory attributes of pork using near-infrared hyperspectral imaging, Analytica Chimica Acta, 2012, 719(10): 30-42.

[6] S. Helling, E. Seidel, and W. Biehlig, Algorithms for spectral color stimulus reconstruction with a seven-channel multispectral camera, in Proc. IS&Ts Proc. 2nd European Conference on Color in Graphics, Imaging and Vision CGIV 2004, Aachen, Germany, Apr. 2004, pp. 254–258.

[7] R. S. Berns and L. A. Taplin, Practical Spectral Imaging Using a Color-Filter Array Digital Camera, July 2006, Final Report, www.artsi.org.

[8] S. A. Mathews, Design and fabrication of a low-cost, multispectral imaging system, Applied optics, 2008, 47(28): 71-6.

[9] S. Han, I. Sato, T. Okabe, and Y. Sato, Fast spectral reflectance recovery using DLP projector, Asian Conference on Computer Vision. (Springer, Berlin Heidelberg), 2010, 323-335.

[10] J. Y. Hardeberg, F. Schmitt, and H. Brettel, Multispectral color image capture using a liquid crystal tunable filter, Optical engineering, 2002, 41(10): 2532-2548.

[11] D Dupont, Study of the reconstruction of reflectance curves based on tristimulus values: comparison of methods of optimization, Color Research and Application, 2002, 27(2): 88-99.

[12] H. Shen, J. Xin, and S. Shao, Improved reflectance reconstruction for multispectral imaging by combining different techniques, Optics express, 2007, 15(15): 5531-5536.

[13] B. Cao, N. Liao, and H. Cheng, Spectral reflectance reconstruction from RGB images based on weighting smaller color difference group, Color Research and Application, 2016.

[14] J. Brauers, N. Schulte, and T. Aach, Multispectral filter-wheel cameras: Geometric distortion model and compensation algorithms, Image Processing, IEEE Transactions on 2008, 17(12): 2368-2380.

[15] H. Shen, H. Wan, and Z. Zhang, Estimating reflectance from multispectral camera responses based on partial least-squares regression, Journal of Electronic Imaging, 2010, 19(2): 020501.

[16] H. Li, Z. Wu, L. Zhang, and J. Parkkinen, SR-LLA: A novel spectral reconstruction method based on locally linear approximation, IEEE International Conference on Image Processing, 2013, 2029-2033.

[17] K. Xiao, Y. Zhu, C. Li, D. Connah, J. M. Yates, and S. Wuerger, Improved method for skin reflectance reconstruction from camera images, Optics express, 2016, 24(13): 14934-14950.

[18] X. Zhang, Q. Wang, J. Li, X. Zhou, Y. Yang, and H. Xu, Estimating spectral reflectance from camera responses based on CIE XYZ tristimulus values under multi-illuminants, Color Research and Application, 2017, 42(1): 68-77.
[19] R. S. Berns, L. A. Taplin, M. Nezamabadi and Y. Zhao, Modifications of a Sinarback 54 camera for spectral and high-accuracy colorimetric imaging: Simulations and experiments, June 2004, www.art-si.org.
[20] J. Liang, X. Wan, Q. Liu, C. Li, and J. Li, Research on filter selection method for broadband spectral imaging system based on ancient murals, Color Research and Application, 2016, 41(6): 585-595.
[21] V. Cheung, S. Westland, and M. Thomson, Accurate estimation of the nonlinearity of input/output response for color cameras, Color Research and Application, 2004, 29(6): 406-412.
[22] D. Connah and J. Y. Hardeberg. Spectral recovery using polynomial models. In Color Imaging: Processing, Hardcopy, and Applications X, volume 5667 of SPIE Proceedings, San Jose, California, 2005, 65–75.
[23] M. Mohammadi, M. Nezamabadi, R. Berns, and L. Taplin, Spectral imaging target development based on hierarchical cluster analysis, in Proceedings of the IS&T/SID 12th Color Imaging Conference (Society for Imaging Science and Technology/Society for Information Display, 2004, 59–64.
[24] M. R. Luo, G. Cui, and B. Rigg, The development of the CIE 2000 colour‐difference formula: CIEDE2000, Color Research and Application, 2001, 26(5): 340-350.

Author Biography

Jinxing Liang received the M.S. degree in graphic communication engineering from Wuhan University in 2015. He is currently pursuing the Ph.D. degree at the Department of printing and packaging, Wuhan University, China. His research interests include spectral imaging and digital preservation of cultural art relics.